Received 25 May 2021; revised 9 September 2021; accepted 27 October 2021.
Date of publication 8 November 2021; date of current version 10 January 2022.

Digital Object Identifier 10.1109/OAJPE.2021.3125900

Detailed Primary and Secondary Distribution System Model Enhancement Using AMI Data

KAREN MONTANO-MARTINEZ[1] (Graduate Student Member, IEEE), SUSHRUT THAKAR[1] (Graduate Student Member, IEEE), SHANSHAN MA[1] (Member, IEEE), ZAHRA SOLTANI[1] (Graduate Student Member, IEEE), VIJAY VITTAL[1] (Life Fellow, IEEE), MOJDEH KHORSAND[1] (Member, IEEE), RAJAPANDIAN AYYANAR[1] (Senior Member, IEEE), AND CYNTHIA ROJAS[2] (Member, IEEE)

[1]School of Electrical, Computer and Energy Engineering, Arizona State University, Tempe, AZ 85287 USA
[2]Arizona Public Service, Phoenix, AZ 85072 USA

CORRESPONDING AUTHOR: V. VITTAL (vijay.vittal@asu.edu)

This work was supported in part by the Advanced Research Projects Agency-Energy under Award DE-AR0001001 and in part by the U.S. Department of Energy, Solar Energy Technologies Office, under Award DE-EE0008773.

ABSTRACT Reliable and accurate distribution system modeling, including the secondary network, is essential in examining distribution system performance with high penetration of distributed energy resources (DERs). This paper presents a highly automated, novel method to enhance the accuracy of utility distribution feeder models to capture their performance by matching simulation results with corresponding field measurements. The method is demonstrated using an actual feeder from an electrical utility with high penetration of DERs. The method proposed uses advanced metering infrastructure (AMI) voltage and derived active power measurements at the customer level, and data acquisition systems (DAS) measurements at the feeder-head, in conjunction with an AC optimal power flow (ACOPF) to estimate customer active and reactive power consumption over a time horizon, while accounting for unmetered loads. The ACOPF uses the measured voltage magnitudes, derived active power measurements, and the feeder head measurements to obtain a complete active power and reactive power capture of the feeder loads. Additionally, the method proposed estimates both voltage magnitude and angle for each phase at the unbalanced distribution substation. The accuracy of the method developed is verified in two stages: by comparing the time-series power flow results obtained from the enhancement algorithm with OpenDSS results and with the field measurements available. The proposed approach seamlessly manages the data available from the optimization procedure through the final model verification automatically.

INDEX TERMS AC optimal power flow (ACOPF), distributed energy resources, distribution system, load modeling, power system modeling, power system measurements, smart grids.

NOMENCLATURE

A. SETS AND INDICES

Ω_N	Set of buses.
Ω_D	Subset of buses with load.
Ω_{AMI_V}	Subset of load buses with AMI voltage information.
Ω_{AMI_D}	Subset of load buses with AMI active power information.
Ω_{D1}	Subset of load buses without AMI information ($\Omega_D - \Omega_{AMI_D}$).
Ω_{PV}	Subset of buses with PV resources.
Ω_{cap}	Subset of buses with capacitor banks.
Ω_{SB}	Set of substation buses.
Ω_L	Set of distribution lines.
Ω_H	Set of feeder-head buses.
Ω_T	Set of distribution transformers.
ψ	Set of phases, i.e., $\{a, b, c\}$.
$\delta(i)$	Set of bus nodes connected to bus i.

B. PARAMETERS

$B_{c,\phi}$	Capacitance of capacitor bank c on phase ϕ.
d_l^D	Gross load at bus l with AMI active power measurements.

P_l^D	AMI active power delivered to bus l.
P_l^R	AMI active power received at bus l.
P_l^{PV}/Q_l^{PV}	AMI active/reactive power produced by the solar PV at bus l.
P_m^{Tr}	No-load loss of transformer m.
P^H/Q^H	DAS active/reactive power data at feeder-head.
$\left\|\hat{V}_{i,\phi}\right\|$	AMI voltage magnitude data at phase ϕ at bus i.
$R_{i,j}^{\phi,p}$	Resistance of distribution line (i,j) between phases ϕ and p.
$X_{i,j}^{\phi,p}$	Reactance of distribution line (i,j) between phases ϕ and p.
$y_{i,j}^{\phi,p}$	Admittance of distribution line (i,j) between phases ϕ and p.
$PF_l^{max/min}$	Maximum/minimum power factor for load l.

C. VARIABLES

$\left\|V_{s,\phi}\right\|/\angle V_{s,\phi}$	Magnitude/angle of voltage at phase ϕ at substation s.
$V_{i,\phi}^r/V_{i,\phi}^{im}$	Real/imaginary part of voltage at phase ϕ at bus i.
$I_{i,\phi}^{r,inj}/I_{i,\phi}^{im,inj}$	Real/imaginary part of injected current at phase ϕ at bus i.
$I_{i,j,\phi}^r/I_{i,j,\phi}^{im}$	Real/imaginary part of line flow current at phase ϕ at bus i.
$P_{s,\phi}^G/Q_{s,\phi}^G$	Active/reactive power output at phase ϕ at substation s.
$P_{l,\phi}^D/Q_{l,\phi}^D$	Active/reactive power at phase ϕ for load l.
$Q_{c,\phi}^C$	Reactive power output of capacitor bank c at phase ϕ.

I. INTRODUCTION

THE increased penetration of distributed energy resources (DERs) – which include renewable energy resources, distributed energy storage, and electric vehicles (EVs) – in the electric grid has resulted in unprecedented changes to power system operation, such as bidirectional power flows and increased voltage fluctuations [1]. As the DER penetration level continues to increase, these issues would further impact the planning and operation of the power distribution systems, increasing the need to monitor and control these resources [2].

Conventionally, distribution systems with just one source at the substation have relied on significant model approximations, avoiding detail extending to the secondary circuits [3], [4]. However, a large share of DERs is located at the distribution system secondary at on-site customer locations, creating the need for a paradigm shift to model distribution systems with more accuracy [5]. Several authors have proposed methods to create approximate models of the secondary circuit [6]–[9]. Nevertheless, an inaccurate model of the secondary network can misrepresent the effects of DERs, resulting in different voltages and incorrect power calculation across the secondary network when conducting power flow analysis [10]. Therefore, reliable and accurate distribution system modeling, including the secondary network and the various components such as load and DER, is essential for distribution system operational analysis while accommodating a high level of DERs.

Due to the recent emphasis on a more accurate representation of the grid, many utilities now have extensive geographic information system (GIS) databases on feeder equipment and conductor segments. Additionally, the utilities are looking to expand the advanced metering infrastructure (AMI) and data acquisition systems (DAS) on the distribution network. By leveraging these data, a high-fidelity feeder model can be developed to address the needs of the utilities to improve distribution system modeling to effectively plan and operate for future smart distribution systems with DERs.

This increase in distribution system observability due to AMI and other emerging sensors has raised the interest in new methods to model the distribution network accurately [11]. A distribution system parameter estimation (DSPE) method using optimal linear regression model and AMI data is proposed in [12]. However, the authors validated their method using a small 66-nodes three-phase test circuit and a single-phase secondary circuit. Additionally, the authors assumed the availability of reactive power measurements or power factors. In reality, this assumption is not always true; therefore, this method portrays an approximate representation of the secondary. Similarly, the authors in [13], [14] use GIS and AMI data to model single-phase loads and high penetration of DERs. However, the authors only modeled loads where measurements exist and assumed a constant power factor for all loads.

A method to estimate the impedance of secondary branches using AMI measurements of voltage and active and reactive power is proposed in [15]. The authors presented an optimization algorithm based on gradient search to calculate the voltage of the upstream node from a measured load. However, this approach requires complete observability of all the loads in the feeder to create an accurate model and may be inaccurate for the feeders with unmetered loads. Another drawback of [11]–[15] is that the authors assumed the source at the feeder-head to be balanced, which does not reflect the unbalanced nature of distribution substations in practical utility feeders.

Reliable and accurate modeling of distribution feeders is important to efficiently manage DERs, especially renewable energy sources, with advanced Volt/VAr optimization and other distribution system automation schemes [12], [16]. This paper focuses on the accurate modeling of unbalanced multi-phase distribution feeder based on the available measurement data, such as AMI voltage and derived active power measurements at the customer level and DAS measurements data. This paper develops a distribution system model enhancement method to model distribution systems, including the secondary network, to capture the feeder performance by

matching feeder model power flow results with corresponding field measurements across the entire feeder. The proposed enhancement method can serve as a benchmark for utilities and academics to improve the model accuracy and reliability of distribution systems for analysis and operation at the utility level with high penetration of DERs. At the same time, the proposed model enhancement method provides a guide for utilities to use automated AMI and DAS measurement to model their distribution feeders with less human intervention.

For the distribution system model enhancement method, this paper proposes an approach based on nonlinear AC optimal power flow (ACOPF) for unbalanced multi-phase distribution systems to increase the system observability and estimate the unmetered loads using available field measurements. The proposed method is based on the rectangular current-voltage (IV) power flow formulation and an extension of the ACOPF model presented in [17]. It is important to note that goal of this paper is different from that of [17]; consequently, the proposed models are different. The approach presented in this paper models the unbalanced multi-phase distribution system in detail and accurately since it considers the impact of distribution lines' mutual impedance and shunt elements on the voltage profile and power loss. Furthermore, compared with the unmetered load estimation function in some commercial software that equally distribute unmetered loads, the proposed ACOPF estimates the unmetered loads by minimizing the norm of the difference between bus voltage magnitudes and the corresponding AMI voltage measurement data. The method developed in this paper seamlessly transfers the available data through the optimization-based method to the final model verification, with limited human intervention.

The effectiveness of the proposed approach is validated on an actual three-phase feeder with high penetration of DERs from an electric utility. The validation is performed in two stages: the first stage compares the power flow solutions obtained in the ACOPF with an OpenDSS (Open Distribution System Simulator) [18] model with the same network, load, and source data – a very good match between the two solutions at this stage of validation highlights that the ACOPF formulation accurately represents the distribution system power flow. The second stage involves comparing the time-series power flow results from the OpenDSS model enhanced using the proposed method with the DAS and AMI measurements in terms of quantities at the substation and the voltages along the feeder at individual residences – a good match at this stage emphasizes that the distribution feeder model is successfully enhanced and accurately matches the actual feeder.

The key contributions of this paper are three-fold:

1) This paper presents a novel computationally efficient method for estimating customer active and reactive power time-series consumption, including unmetered loads, using AMI voltage and derived power measurements available at some customer locations along the feeder. The reactive power for each premise is calculated instead of assuming a constant power factor for all the loads in the feeder, providing a more accurate feeder model.
2) An unbalanced substation model is proposed and implemented to capture the unbalanced nature of distribution substations in practical utility feeders. For phases at the substation with no available voltage measurements, both the voltage magnitude and angle are estimated.
3) This method provides a complete power flow solution, including the secondary circuit representation, using sparse measurements along a feeder, extending the observability and planning capabilities of the feeder under study.

This paper is structured as follows. Section II describes the modeling data resources available at the utility level and their implementation in the development of a detailed distribution system model. Section III presents the proposed distribution system model enhancement algorithm, the data implementation to create the input data for the algorithm, the formulation of the proposed ACOPF approach, the enhancement algorithm output, and its simulation capabilities. Section IV presents the validation between the enhancement algorithm power flow output and OpenDSS power flow and the validation between the enhancement algorithm power flow output and the field measurements. Section V presents some feeder characteristics derived from the enhanced feeder model developed. Section VI provides a discussion, and Section VII concludes the paper.

II. MODELING DATA RESOURCES

The objective of the proposed model enhancement method is to obtain an accurately detailed distribution system model to capture the performance of the feeder by matching simulation results with corresponding field measurements.

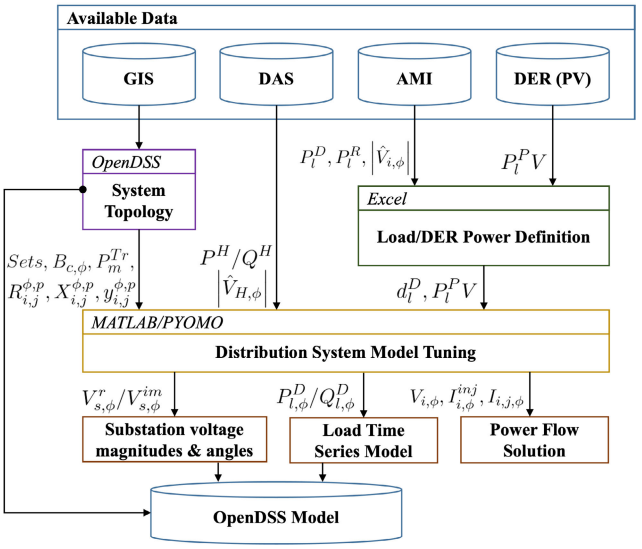

FIGURE 1. Modeling data resources for distribution system model enhancement.

Fig. 1 illustrates the modeling data resources for the proposed distribution system model enhancement method. The GIS database contains conductor details and the latitude and the longitude of both endpoints of all the circuit sections, including the secondary network. Additionally, equipment ratings of transformers and capacitors and locations of the system elements such as loads, and PV units are available. These data are used to create the distribution system topology, including load allocation, using the approach presented in [19] and [20]. The DAS database contains hourly feeder-head measurements, which are used for the construction and validation of the distribution feeder model.

The AMI database contains measurements of energy *(kWh)* from PV (production) meters and load (billing) meters. These measurements are given as aggregated values every 15 minutes or each hour, depending on the meter. The hourly average active power *(kW)* (henceforth termed "active power" in this paper) is derived for each meter by aggregating the measurements of energy consumption for one hour. The AMI database includes voltage magnitude measurements from various load meters given each 15 minutes. These considerations are taken after discussions with the utility, who provided the measurements and information about how they manage their data.

There are two cases for load modeling: metered loads (Ω_{AMI_D}) and unmetered loads (Ω_{D1}). For the metered loads, the active power definition is based on the AMI measurements of the derived active power available at that premise. Fig. 2 shows the metering infrastructure installed at a typical metered premise, where the household has separate meters for PV production and billing. The load active power definition for metered loads is represented by the gross load $\left(d_l^D,\ l \in \Omega_{AMI_D}\right)$, which is the total active power demand at a household. The production meter measurements are used to derive the active power produced by the PVs $\left(P_l^{PV},\ l \in \Omega_{PV}\right)$ and to define the PV generation. The billing meter is a bi-directional meter whose measurements are used to derive the power delivered by the utility to the customer (P_l^D) and the power received by the utility from the customer (P_l^R). Hence, (1) is used to estimate the gross load of a metered premise.

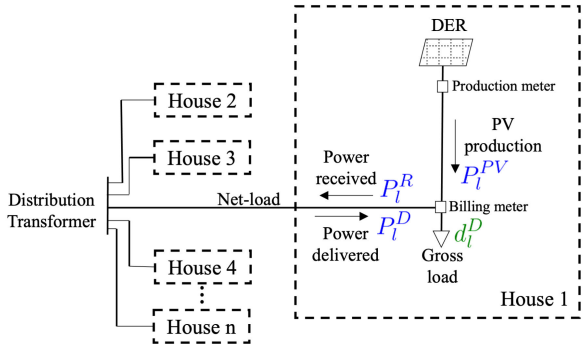

FIGURE 2. Metering infrastructure at a typical premise: available measurements are in blue, estimated values are in green.

$$d_{l,\phi}^D = P_{l,\phi}^D - P_{l,\phi}^R + P_{l,\phi}^{PV}, \quad \forall\, l \in \Omega_{AMI_D}\ ,\ \phi \in \psi(l) \qquad (1)$$

On the other hand, the power definition for unmetered loads ($P_l^D,\ l \in \Omega_{D1}$) is set as a variable to be estimated by the enhancement method.

The proposed method relies on the following assumptions regarding the available data:

1) The secondary network topology is assumed to be known. If the topology is unknown, the approach presented in [19] can be used to estimate the system topology.
2) The following feeder-head measurements are assumed to be available and accurate: feeder-head total three-phase active power (P^H) and reactive power (Q^H) and feeder-head voltage magnitude $\left(\left|\hat{V}_{i,\phi}\right|,\ i \in \Omega_H\right)$ for at least one phase, ϕ.
3) The gross load of the metered loads $\left(d_l^D,\ l \in \Omega_{AMI_D}\right)$ is assumed to be available or derivable from the AMI measurements available in the system.
4) The active/reactive powers of the DERs (P_l^{PV}/Q_l^{PV}, $l \in \Omega_{AMI}$) are assumed to be available from the AMI measurements available in the system. In the system considered, the reactive power of the DERs ($Q_l^{PV},\ l \in \Omega_{AMI}$) is assumed to be zero - at present, all DERs in the system operate at unity power factor and do not participate in any reactive power support of the system.
5) Load voltage measurements $\left(\left|\hat{V}_{i,\phi}\right|, \forall\, i \in \Omega_{AMI_V}\right)$ are assumed to be available for some of the loads. However, it is not necessary to have these voltage measurements for the same loads as in Assumption 3.
6) The field measurements available are assumed to be accurate.

The system topology, feeder-head measurements, load voltage measurements available, DERs power definition, and the initial power definition of the loads are processed in MATLAB to create the input data to the optimization-based method. The ACOPF based on an IV formulation for distribution system model enhancement is programmed using Pyomo, which is a Python-based, open-source optimization modeling language [21], [22]. IPOPT is used as the nonlinear solver for the proposed ACOPF approach [23]. The output from the distribution system model enhancement includes time-series substation voltage magnitudes and angles, load active and reactive power demand, and power flow solution. The power flow from the resulting enhanced distribution system model is compared with the power flow from OpenDSS to validate the accuracy of the proposed optimization-based method.

III. DISTRIBUTION SYSTEM MODEL ENHANCEMENT ALGORITHM

This section presents the formulation of the proposed method, the data implementation to create the input data for the algo-

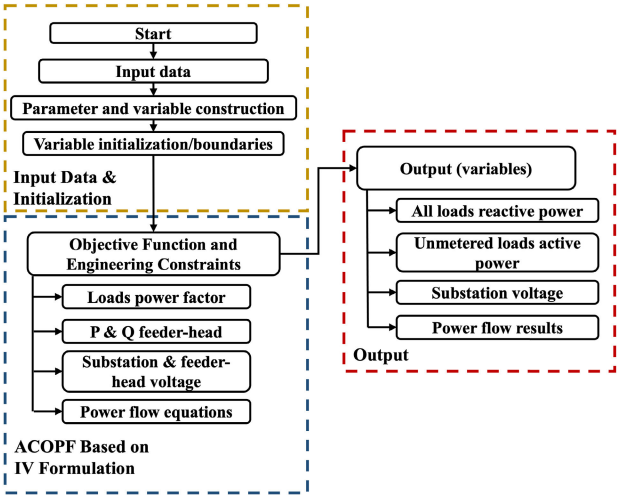

FIGURE 3. Flowchart for distribution system model enhancement algorithm.

rithm, the formulation of the proposed ACOPF approach, the algorithm output and simulation capabilities. A flowchart explaining the optimization technique proposed is summarized in Fig. 3.

A. INPUT DATA AND INITIALIZATION

The input data contains the feeder topology information and AMI/DAS measurement data. The feeder topology data includes the information to create the subset of buses with load, PV, capacitor and transformers, and impedance information of each distribution line. The AMI measurement data includes the energy measurements (kWh) used to derive the hourly active power (kW) for the metered load. The AMI database also includes voltage magnitude measurements for some loads in the feeder. The DAS measurement data includes total active/reactive power at the feeder-head and the voltage magnitude of one phase. The detailed procedure for creating the input data is described in Algorithm 1.

Most nonlinear solvers only find local optimal solutions for nonconvex problems [24]. Therefore, a good initialization is essential to find a solution that meets the problem requirements. After the input data is created, the parameters and variables are defined. The parameters are listed under the assumptions in Section II. The variables in the enhancement algorithm include bus voltages, unmetered load active power definitions, load reactive power definitions, bus injection currents, line flow currents, reactive power production of capacitors, and per phase substation active/reactive powers and voltages. The bus voltage magnitudes, bus injection currents, and line flow currents are initialized using a flat start: balanced voltages of magnitude 1.0 $p.u.$ and line currents of magnitude 0 $p.u.$ for all the buses and lines. The active powers for unmetered loads may be initialized based on the type of load (residential/commercial/industrial) and the feeder location or based on the active power measurements from other metered loads available. However, this initialization can be adjusted without loss of generality, knowing whether the load is residential, commercial, or industrial. The reactive power for all the loads is initialized using a constant power factor of 0.9 lagging. The reactive power for all the capacitor banks is initialized using a terminal voltage of 1 p.u. and the nominal capacitance using (9). The substation per phase active/reactive powers are initialized using one-third of the total three-phase measurement at the feeder-head. The substation voltage is initialized at the same voltage as the feeder-head measurement.

Algorithm 1 Input Data Creation

Input: Feeder topology and AMI/DAS measurements.

Output: Distribution system model enhancement algorithm input data.

1: Read feeder topology and line impedances ($R_{i,j}^{\phi,p}, X_{i,j}^{\phi,p}, y_{i,j}^{\phi,p}$).
2: Create topology sets (Ω_N, Ω_D, Ω_{PV}, Ω_{cap}, Ω_{SB}, Ω_L, Ω_H, Ω_T).
3: Read equipment information ($B_{c,\phi}, P_m^{Tr}$).
4: Read DAS measurements (P^H, Q^H, $|\hat{V}_{H,\phi}|$).
5: Read AMI measurements of energy (kWh) and voltage magnitude $\left(\left|\hat{V}_{i,\phi}\right|\right)$.
6: Create sets of buses with measurements (Ω_{AMI_V}, Ω_{AMI_D}).
7: Write line/transformer data ($R_{i,j}^{\phi,p}, X_{i,j}^{\phi,p}, y_{i,j}^{\phi,p}$) for the algorithm.
8: **for** $hour = 1$ to 24 **do**
9: Derive hourly active power measurements at each meter by aggregating the measurements of energy consumption (P_l^D, P_l^R, $P_l^{PV}, \forall\, l \in \Omega_{AMI_D}$).
10: Derive the gross load $\left(d_l^D,\ l \in \Omega_{AMI_D}\right)$ using (1).
11: Read the PV active power ($P_l^{PV},\ l \in \Omega_{PV}$).
12: Write gross load and PV active power data.
13: Write equipment data ($B_{c,\phi}, P_m^{Tr}$) for the algorithm.
14: Write voltage measurement data $\left(\left|\hat{V}_{i,\phi}\right|\right)$ for the algorithm.
15: **end for**

B. ENHANCEMENT ALGORITHM: ACOPF BASED ON IV FORMULATION

This subsection formulates the optimization-based problem proposed for the distribution system model enhancement method as an ACOPF formulation based on a three-phase IV model for unbalanced distribution networks with mutual impedance, which is more appropriate for distribution networks [17], [25]. The IV formulation solves a linear system of equations without decomposition, unnecessary constraints, or omissions, and it may be computationally easier to solve than the traditional quadratic power flow formulations [24]. The ACOPF presented in this paper co-optimizes active and reactive power along the distribution feeder. The nonlinear formulation is carried out in rectangular coordinates. The proposed model enhancement algorithm reads the input data and

initial values of the variables and transfers the information through the engineering constraints while optimizing the system performance according to the objective function, shown in Fig. 3.

The objective of this formulation is to minimize the norm of the difference between bus voltage magnitudes and the corresponding AMI voltage measurement data. Since the rectangular representation of currents and voltages is considered, the square of the voltage magnitude is used, which is equal to the summation of the squares of the real part and imaginary parts of the voltage. The formulation of the objective function is shown in (2).

$$\min \sum_{i\in\Omega_{AMI_V}} \sum_{\phi\in\psi} \left({V^r_{i,\phi}}^2 + {V^{im}_{i,\phi}}^2 - \left|\hat{V}_{i,\phi}\right|^2 \right)^2 \tag{2}$$

Let i and j be the indices of the sending and receiving buses of a line (i, j). For line flow equations, the mathematical relation between the voltage difference between the two buses (i, j) for each phase (ϕ) of a line and the current flow for each phase of a line in an unbalanced three-phase distribution system are expressed in (3)-(4).

$$\begin{aligned} V^r_{i,\phi} - V^r_{j,\phi} = &\sum_{p\in\psi} R^{\phi,p}_{i,j} \left(I^r_{i,j,p} + \frac{1}{2} \sum_{k\in\psi} y^{p,k}_{i,j} V^{im}_{i,k} \right) \\ &- \sum_{p\in\psi} X^{\phi,p}_{i,j} \left(I^{im}_{i,j,p} - \frac{1}{2} \sum_{k\in\psi} y^{p,k}_{i,j} V^r_{i,k} \right), \\ &\forall (i,j) \in \Omega_L, \phi \in \psi \end{aligned} \tag{3}$$

$$\begin{aligned} V^{im}_{i,\phi} - V^{im}_{j,\phi} = &\sum_{p\in\psi} R^{\phi,p}_{i,j} \left(I^{im}_{i,j,p} - \frac{1}{2} \sum_{k\in\psi} y^{p,k}_{i,j,} V^r_{i,k} \right) \\ &- \sum_{p\in\psi} X^{\phi,p}_{i,j} \left(I^r_{i,j,p} + \frac{1}{2} \sum_{k\in\psi} y^{p,k}_{i,j} V^{im}_{i,k} \right), \\ &\forall (i,j) \in \Omega_L, \phi \in \psi \end{aligned} \tag{4}$$

The real and imaginary parts of the current injection constraint are defined using (5) and (6), respectively.

$$I^{r,inj}_{i,\phi} = \sum_{j\epsilon\delta(i)} I^r_{i,j,\phi}, \quad \forall i \in \Omega_N, \phi \in \psi \tag{5}$$

$$I^{im,inj}_{i,\phi} = \sum_{j\epsilon\delta(i)} I^{im}_{i,j,\phi}, \quad \forall i \in \Omega_N, \phi \in \psi \tag{6}$$

The active power balance constraint is defined in (7). The reactive power balance constraint is defined in (8), considering capacitor output $(Q_{c,\phi})$.

$$\begin{aligned} &V^r_{i,\phi} I^{r,inj}_{i,\phi} + V^{im}_{i,\phi} I^{im,inj}_{i,\phi} \\ &= \sum_{\substack{\forall s\in\Omega_{SB} \\ s=i}} P^G_{s,\phi} - \sum_{\substack{\forall m\in\Omega_T \\ m=i}} P^{Tr}_{m,\phi} \\ &\quad - \sum_{\substack{\forall l\in\Omega_{D1} \\ l=i}} P^D_{l,\phi} + \sum_{\substack{\forall l\in\Omega_{PV} \\ l=i}} P^{PV}_{l,\phi} - \sum_{\substack{\forall l\in\Omega_{AMI_D} \\ l=i}} d^D_{l,\phi}, \end{aligned}$$

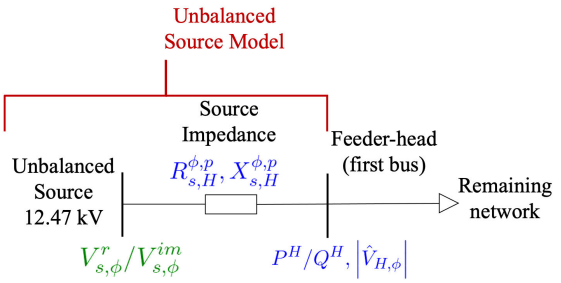

FIGURE 4. Source and feeder-head representation in the proposed framework: available measurements are in blue, estimated values are in green. Three independent single-phase voltage sources are implemented in the unbalanced source bus to model an unbalanced circuit.

$$\forall i \in \Omega_N, \phi \in \psi \tag{7}$$

$$\begin{aligned} &V^{im}_{i,\phi} I^{r,inj}_{i,\phi} - V^r_{i,\phi} I^{im,inj}_{i,\phi} \\ &= \sum_{\substack{\forall s\in\Omega_{SB} \\ s=i}} Q^G_{s,\phi} + \sum_{\substack{\forall c\in\Omega_{cap} \\ c=i}} Q^C_{c,\phi} \\ &\quad - \sum_{\substack{\forall l\in\Omega_D \\ l=i}} Q^D_{l,\phi} + \sum_{\substack{\forall l\in\Omega_{PV} \\ l=i}} Q^{PV}_{l,\phi}, \quad \forall i \in \Omega_N, \ \phi \in \psi \end{aligned} \tag{8}$$

where the reactive power output of a connected capacitor is modeled using a constant capacitance model. Therefore, the reactive power is expressed as follows:

$$Q^C_{c,\phi} = B_{c,\phi} \left({V^r_{c,\phi}}^2 + {V^{im}_{c,\phi}}^2 \right), \quad \forall c \in \Omega_{cap}, \phi \in \psi \tag{9}$$

The substation model shown in Fig. 4 is proposed and implemented to capture the unbalanced nature of distribution substations in practical utility feeders (Section III-C). The voltage magnitude limits at the feeder-head are expressed in (10).

$$V^{min\,2}_{i,\phi} \leq {V^r_{i,\phi}}^2 + {V^{im}_{i,\phi}}^2 \leq V^{max\,2}_{i,\phi}, \ \forall i \in \Omega_H, a \neq \phi \in \psi \tag{10}$$

The upper and lower bounds in (10) are established according to the feeder-head available measurements of voltage $\left(\left|\hat{V}_{i,\phi}\right|, \ i \in \Omega_H\right)$. The feeder modeled in this paper has available hourly measurements of voltage magnitude at the feeder-head for phase a $\left(\left|\hat{V}_{H,a}\right|\right)$, which is considered a parameter for this phase by the model enhancement algorithm. On the other hand, the voltage magnitude at the feeder-head of phases b and c are calculated individually by the algorithm proposed. Hence, the voltage magnitudes of phases b and c are allowed a deviation of 2% from the measured phase a voltage via (10) – the limits $V^{min}_{i,\phi}$ and $V^{max}_{i,\phi}$ should be set based on the available measurements for the feeder modeled. For a distribution feeder with separate voltage magnitude measurements available for all three phases ϕ, all three feeder-head voltages $\left(\left|\hat{V}_{H,\phi}\right|, \ \phi \in \psi\right)$ would be considered as parameters.

The voltage magnitude limits for the source behind the equivalent impedance are expressed in (11). The voltage

magnitudes of the three phases for the source are calculated individually by the algorithm proposed with a maximum deviation of 2.5% from $\left|\hat{V}_{H,a}\right|$. The limits in (11) are determined based on the order of magnitude of the source impedance and to facilitate higher feasibility for the optimization.

$$V_{s,\phi}^{min} \leq \left|V_{s,\phi}\right| \leq V_{s,\phi}^{max}, \quad \forall s \in \Omega_{SB},\ \phi \in \psi \tag{11}$$

The real and imaginary parts of the source voltage are given by (12) - (13), respectively.

$$V_{s,\phi}^{r} = \left|V_{s,\phi}\right| \cos\left(\angle V_{s,\phi}\right), \quad \forall s \in \Omega_{SB},\ \phi \in \psi \tag{12}$$

$$V_{s,\phi}^{im} = \left|V_{s,\phi}\right| \sin\left(\angle V_{s,\phi}\right), \quad \forall s \in \Omega_{SB},\ \phi \in \psi \tag{13}$$

where the voltage angles are limited using (14). The limits in (14) are set to allow the consideration of an unbalanced source while still maintaining a roughly 120° angle difference between any two phases.

$$\angle V_{s,\phi}^{min} \leq \angle V_{s,\phi} \leq \angle V_{s,\phi}^{max}, \quad \forall s \in \Omega_{SB},\ \phi \in \psi \tag{14}$$

The reactive power of each load is limited by its maximum and minimum power factor using (15)-(16).

$$d_{l,\phi}^{D}\sqrt{\left(\frac{1}{(PF_{l}^{max})^2}-1\right)} \leq Q_{l,\phi}^{D} \leq d_{l,\phi}^{D}\sqrt{\left(\frac{1}{(PF_{l}^{min})^2}-1\right)}, \quad \forall l \in \Omega_{AMI_D},\ \phi \in \psi \tag{15}$$

$$P_{l,\phi}^{D}\sqrt{\left(\frac{1}{(PF_{l}^{max})^2}-1\right)} \leq Q_{l,\phi}^{D} \leq P_{l,\phi}^{D}\sqrt{\left(\frac{1}{(PF_{l}^{min})^2}-1\right)}, \quad \forall l \in \Omega_{D1},\ \phi \in \psi \tag{16}$$

where PF_{l}^{max} and PF_{l}^{min} are the limits on the power factors of the loads. These limits should be selected to be suitable for the modeled feeder. Since DAS measurements of the total three-phase active and reactive power are available at the feeder-head, the summation of power injections at the different phases at the feeder-head is assumed to be equal to the measured value.

$$\sum_{\phi \in \psi}\left(V_{h,\phi}^{r} I_{h,\phi}^{r,inj} + V_{h,\phi}^{im} I_{h,\phi}^{im,inj}\right) = P^{H}, \quad \forall h \in \Omega_{H} \tag{17}$$

$$\sum_{\phi \in \psi}\left(V_{h,\phi}^{im} I_{h,\phi}^{rinj} - V_{h,\phi}^{r} I_{h,\phi}^{im,inj}\right) = Q^{H}, \quad \forall h \in \Omega_{H} \tag{18}$$

C. ALGORITHM OUTPUT AND SIMULATION CAPABILITIES

The algorithm developed solves a three-phase distribution system power flow problem. The power flow can be solved in standard single snapshot mode and daily variable time-interval mode. The time interval can be any time period. The feeder model developed in this paper is solved for each day using 24-hourly steps. When the power flow is solved, the losses, voltages, flows, and other information are available for the total system and each element.

For each instant in time, the algorithm automatically exports the power flow solution of the system, as well as the active and reactive power definition of the loads ($P_{l,\phi}^{D}/Q_{l,\phi}^{D}, \forall l \in \Omega_D$), distributed generators output ($P_{l}^{PV}, \forall l \in \Omega_{PV}$), and source voltage magnitudes and angles ($\left|V_{s,\phi}\right|/\angle V_{s,\phi}, \phi \in \psi$), as shown in Fig. 3. These data are then used to complete the OpenDSS model, as explained in the next section.

D. OpenDSS OPTIMAL FEEDER MODEL

An OpenDSS time-series feeder model is constructed based on the optimization algorithm results as the output of the feeder model enhancement method. This enhanced OpenDSS model is then used for any further studies involving the distribution feeder modeled. For this time series model, the voltage source and each load and PV generator follow hourly profiles obtained from the enhancement algorithm and transferred to OpenDSS through shape files. The profiles are created for active and reactive power for each load/PV generator and the voltage magnitude of each of the three phases at the unbalanced source. The loads are modeled using constant P and constant Q to preserve the power flow obtained from the enhancement algorithm. The solar PV units are modeled as electronically coupled generators using the current-limited constant kW OpenDSS model and based on the AMI measurements.

OpenDSS models a three-phase voltage source as a balanced voltage source behind a Thévenin equivalent impedance. However, balanced sources at the distribution network are not accurate enough to represent the unbalanced voltages common in practical utility feeders [26]. Therefore, to model the unbalanced distribution system more accurately, the optimization-based method proposed implements three independent single-phase voltage sources to model an unbalanced substation source, as shown in Fig. 4. Since the feeder-head measurement of voltage is available only for the magnitude of one phase $\left(\left|\hat{V}_{H,a}\right|\right)$ for the modeled feeder, the feeder-head voltage for the remaining phases and the source voltages are obtained by the ACOPF formulation proposed.

The voltage source and feeder-head representation shown in Fig. 4 and used in the algorithm corresponds to the Thévenin equivalent impedance representing the substation transformer and the sub-transmission/transmission system. In the enhancement algorithm, this source impedance is represented as a line with no capacitance ($R_{s,H}^{\phi,p}$, $X_{s,H}^{\phi,p}$, $\phi, p \in \psi$). As a result, three shapefiles corresponding to the voltage magnitude for each of the three phases at the substation are created for the OpenDSS model. On the other hand, while the enhancement algorithm provides the voltage angle for each phase at each step of the time series simulation, OpenDSS does not allow voltage source angle variation through shape-

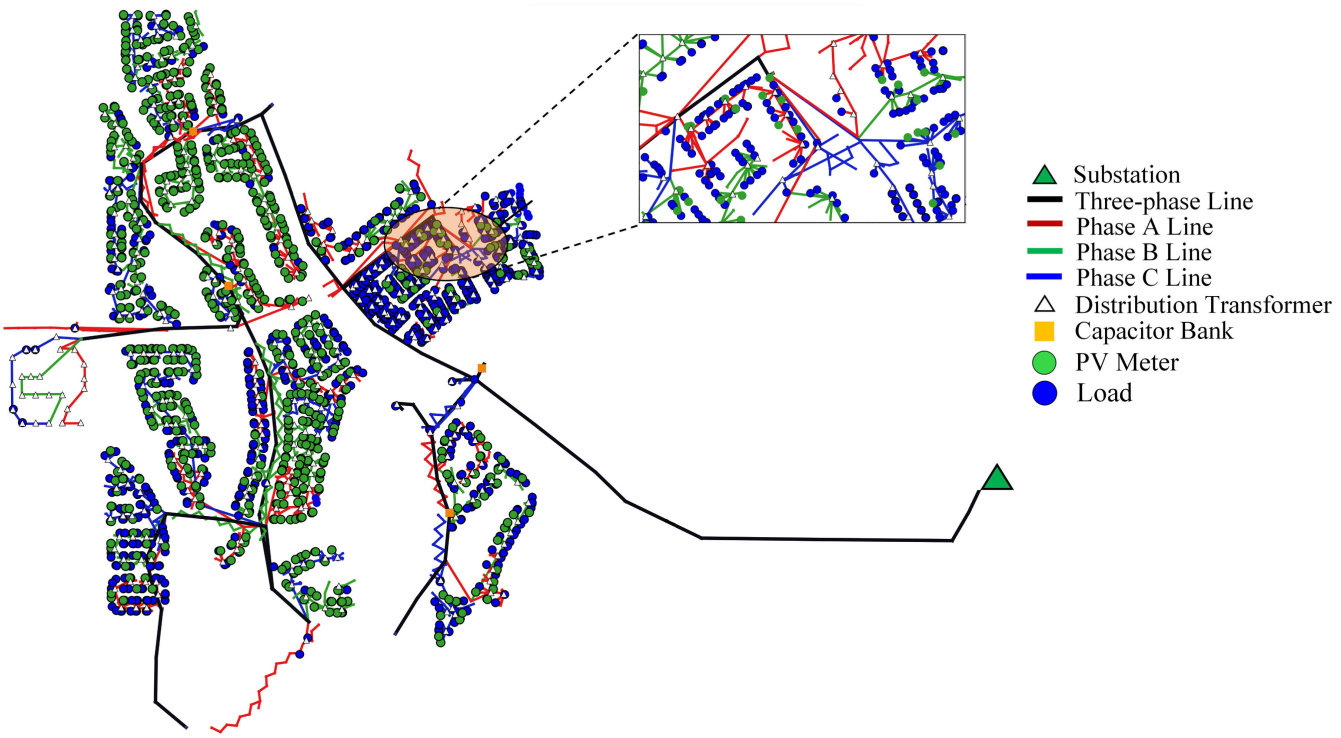

FIGURE 5. **Arizona utility feeder circuit diagram with all the elements.**

files. Therefore, unbalanced angles are defined at each of the three single-phase sources at the substation bus and hence are kept constant while solving a time series power flow problem in OpenDSS.

Monitors are then set at the feeder-head bus and every load bus in the system to capture the results of voltages and powers at those points. Then, the results of the monitors are compared against the AMI measurements at the loads and DAS measurements at the feeder-head to validate the system. The model validation is discussed in Section IV.

IV. MODEL VALIDATION: UTILITY FEEDER RESULTS

This section presents the validation between the enhancement algorithm power flow output and OpenDSS power flow and the validation between the enhancement algorithm power flow output and the field measurements.

The proposed algorithm is tested on an actual $12.47\,kV$, nine $km-$long utility feeder in Arizona that serves residential customers. Fig. 5 shows the circuit diagram of the feeder with all its elements. The peak net load on the feeder was $7.35\,MW$ on $07/15/2019$. The feeder has one of the highest PV penetrations among the utility's operational feeders, with $3.8\,MW$ of residential rooftop PV installed. Hence, a penetration level of more than 200% compared to the feeder total gross load ($3.8\,MW$ total solar PV generation/$1.6\,MW$ total gross load) is observed during peak solar PV production hours. The OpenDSS model for this feeder has an unbalanced $69/12.47\,kV$ source representing the substation, 7864 buses, 1790 primary sections, 5782 secondary sections, 371 distribution transformers, four capacitor banks of $1.2\,MVAr$ rating each, 1737 loads, and 766 PV units. There are 784 PV (production) and 1652 load (billing) meters installed on the system, and 1194 meters of these also report voltage magnitudes.

Since the modeled feeder is a residential feeder in Arizona, and since a typical household peak load in Arizona lies between $4-7\,kW$ due to the need for air conditioning, a value of $5\,kW$ is chosen to initialize the unmetered loads' active power. For loads connected to a distribution transformer with other measured loads, similar values as those measured loads are used to initialize their active power instead. For the feeder modeled, the limits of the power factors of the loads (PF_l^{max} and PF_l^{min}) are selected to include the power factor at the feeder-head - obtained from the measurements of active and reactive power at the feeder-head for a time-step. Most solar PV units installed on this feeder operate with unity power factor in practice. Therefore, the reactive power exchanged by the solar PV units ($Q_{l,\phi}^{PV}$) with the rest of the distribution system is set to zero in (8).

The presented optimization algorithm is implemented using Pyomo (version 5.7) and solved using IPOPT solver (version 3.11.1.). The optimizations are carried out on a computer with a 4-core 1.8 GHz Intel Core i7-8550U CPU and 16 GB of RAM. On this machine, optimizing the feeder model for one snapshot (once loaded) requires approximately 32 seconds and involves 134,623 variables and 133,264 equality and inequality constraints.

A. ALGORITHM-OpenDSS POWER FLOW COMPARISON

This section presents the validation between the enhancement algorithm power flow output and OpenDSS power flow. To perform the validation, the actual historical feeder peak load snapshot on 07/15/2019 (high load and relatively low PV) is chosen for the analysis. The resultant load active and reactive powers, the per unit voltages at the three phases of the source, and the input data such as the network topology and parameters, capacitors, and solar PV generation are implemented in an OpenDSS model. Then, the power flow obtained from the optimization algorithm and the power flow solution obtained from OpenDSS for the same operating point are compared to validate the representation of the power flow equations in the optimization algorithm. A good match between the two would imply that the optimization algorithm accurately represents the power flow equations.

For this comparison, the consumed/produced active and reactive power for each element in the feeder are calculated from the algorithm power flow solution and compared against the corresponding power element losses exported from OpenDSS. The consumed/produced active and reactive power for each element in the feeder is calculated according to the type of the element.

For all the lines (Ω_L) in the feeder, where i and j are the sending and receiving bus indices, the active and reactive power consumption (inductive lines) and reactive power production (capacitive underground lines) are calculated as the power difference between the sending and receiving ends.

Similarly, for all the transformers (Ω_T) in the feeder, the active and reactive power consumption is calculated as the power difference between the sending and receiving ends plus the no-load loss (P_m^{Tr}, $\forall\, m \in \Omega_T$), which represents a resistive branch in parallel with the magnetizing inductance. For all the capacitors (Ω_{cap}), (9) is used to calculate the reactive power injections.

The algorithm uses (7)-(8) to calculate the load active power $\left(d_l^D,\ \forall l \in \Omega_{AMI_D};\ P_l^D,\ \forall l \in \Omega_{D1}\right)$ and reactive power ($Q_l^D,\ \forall l \in \Omega_D$). The active and reactive power production from the solar PV units ($P_l^{PV},\ Q_l^{PV},\ \forall l \in \Omega_{PV}$) are input from the AMI data and are held to be the same between the optimization algorithm and the OpenDSS model.

The source active and reactive powers are calculated by using the receiving end (feeder-head end) of the line that connects the substation with the feeder-head, that is,

$$P_{s,\phi}^G = V_{H,\phi}^r I_{s,H,\phi}^r + V_{H,\phi}^{im} I_{s,H,\phi}^{im}, \quad \phi \in \psi \tag{19}$$

$$Q_{s,\phi}^G = V_{H,\phi}^{im} I_{s,H,\phi}^r - V_{H,\phi}^r I_{s,H,\phi}^{im}, \quad \phi \in \psi \tag{20}$$

The comparison between the consumed/produced active and reactive power for each type of element in the optimization algorithm power flow solution and the corresponding power element losses exported from OpenDSS model during a single snapshot (historical feeder load peak) is shown in TABLE 1. For instance, the row corresponding to "Lines" lists the total power consumed by all the lines in the system for both the optimization algorithm and the OpenDSS model

TABLE 1. Comparison of active and reactive power from power flow solution for a single snapshot.

Component	Proposed Algorithm		OpenDSS		% Error	
	P (MW)	Q (MVar)	P (MW)	Q (MVar)	P	Q
Source	-5.978	-0.522	-5.979	-0.523	0.01	0.13
Lines	0.083	-0.423	0.083	-0.423	0.17	0.06
Capacitors	0.000	-1.261	0.000	-1.260	0.00	0.01
Loads	7.725	2.166	7.728	2.167	0.03	0.02
Transformers	0.073	0.040	0.070	0.040	2.95	0.01
PVs	-1.903	0.000	-1.903	0.000	0.00	0.00

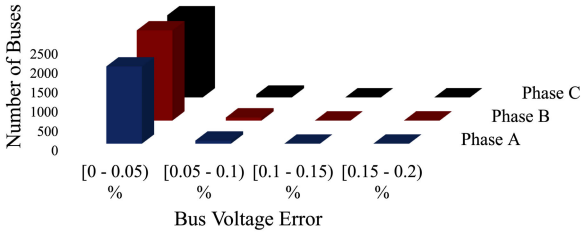

FIGURE 6. Bus voltage magnitude error per phase between enhancement algorithm power flow and OpenDSS solution for a single snapshot for the historical feeder load peak hour for the modeled feeder.

power flow, as well as the percentage difference between both. The corresponding comparisons match under 0.13% error (except for the transformer active power comparison, which has an error of 2.95%, equivalent to $3kW$ – still relatively low considering that this 3 kW difference is the combined losses for all the distribution transformers).

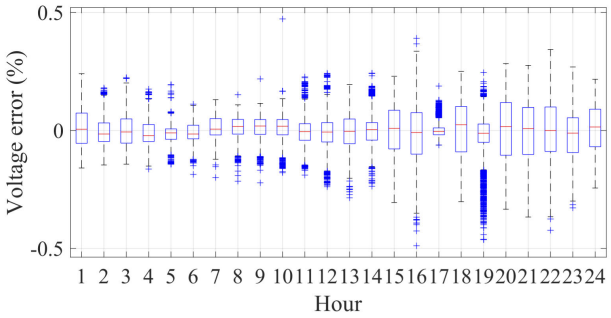

FIGURE 7. Voltage errors between OpenDSS and the optimization-based algorithm for different hours of a single day (historical feeder load peak day) for the modeled feeder. The red line in the middle in each case indicates the median error, the box indicates the interquartile range, and the whiskers are defined as 1.5 times the interquartile range away from the box.

For the same snapshot (historical feeder load peak), Fig. 6 shows a per phase comparison of the voltage magnitude of all the buses (Ω_N) between the enhancement algorithm and OpenDSS solution. Fig. 7 shows the voltage errors between OpenDSS and the enhancement algorithm for time-series analysis (using the same load demands, solar PV generation, and source voltage) for different hours of a single day

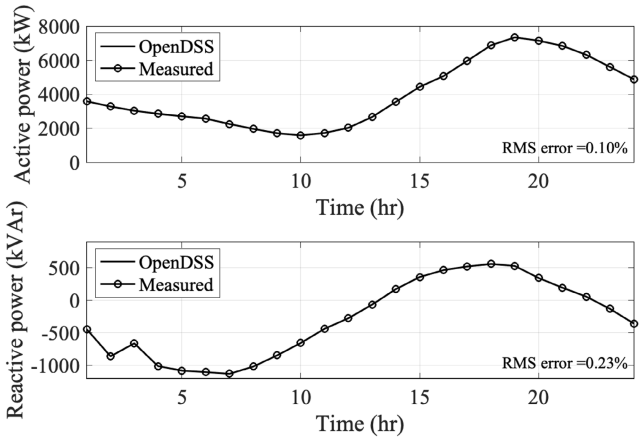

FIGURE 8. **Active and reactive power feeder-head comparison between the enhanced OpenDSS model and DAS measurements for the historical feeder load peak day.**

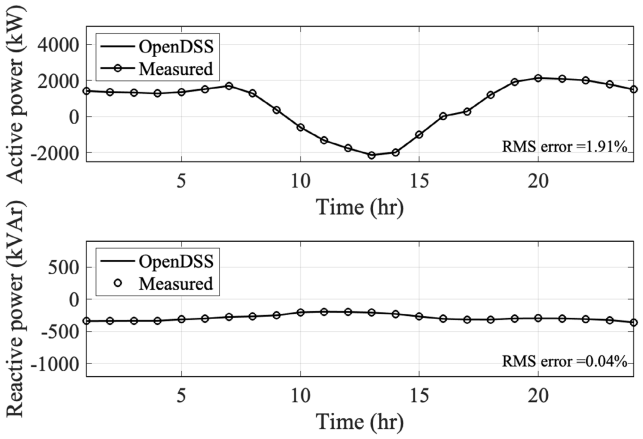

FIGURE 9. **Active and reactive power feeder-head comparison between the enhanced OpenDSS detailed model and DAS measurements for the maximum generation condition day.**

(historical feeder load peak day). The low errors show that the enhancement algorithm models the power flow constraints correctly and that the results obtained from the enhancement algorithm match closely with the electrical model and assumptions employed in a state-of-the-art distribution system power flow solver such as OpenDSS. Therefore, the OpenDSS time-series feeder model constructed based on the optimization algorithm results reflects the enhanced feeder model accurately and can be used for further studies involving the distribution feeder modeled.

B. ENHANCED DISTRIBUTION FEEDER MODEL VALIDATION

This section presents the validation between the enhancement algorithm power flow output and the field measurements. Two days corresponding to the actual historical feeder load peak on 07/15/2019 (high load and relatively low PV) and the maximum generation condition on 03/15/2019 (high PV) were chosen for the analysis to validate the feeder enhancement algorithm power flow.

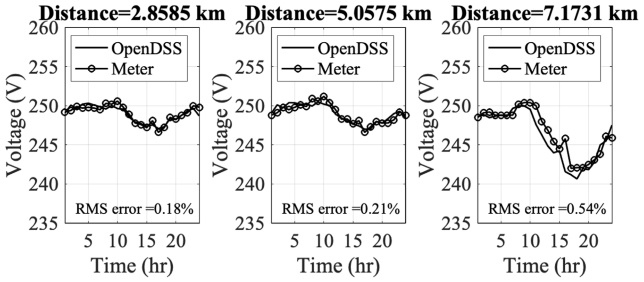

FIGURE 10. **Voltage comparison results between OpenDSS and AMI data for some premises along the feeder for the historical feeder load peak day.**

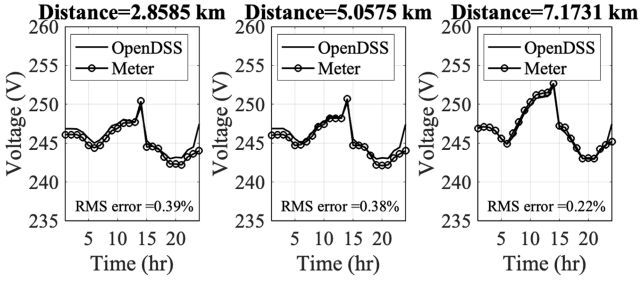

FIGURE 11. **Voltage comparison results between OpenDSS and AMI data for some premises along the feeder for the maximum generation condition day.**

Using the OpenDSS time-series feeder model constructed based on the optimization algorithm results from the previous sections, a time series power flow yielded a good match with the measured values. The OpenDSS feeder-head active and reactive powers are compared with the corresponding feeder-head measurements for both days in Fig. 8 and Fig. 9. For the historical feeder load peak day, the feeder-head active and reactive powers have root mean square (*RMS*) errors over a day of 0.104% and 0.234%, respectively. For the day with the maximum generation, the feeder-head active and reactive powers have *RMS* errors over a day of 1.897% and 0.0493%, respectively. The small *RMS* errors imply that the powers at the feeder-head from the enhanced OpenDSS time-series feeder model power flow accurately represents the field-measured values. Note that the reactive power along the feeder is completely calculated by the optimization-based technique by minimizing the objective function (2) and under the constraints of Section III-B, as there are no reactive power measurements available at any point along the feeder aside from the feeder-head values. The active power is varied for a subset of the loads (Ω_{D1}) by the enhancement algorithm; therefore, a small error at the feeder-head active power indicates the model successfully being tuned to represent the measurements and, by proxy, the actual feeder status.

As further validation, the voltages at the premises along the feeder where AMI measurements are available are compared against these measurements. The comparison between the AMI measurements and model voltages for three representative meters at different locations along the feeder for the

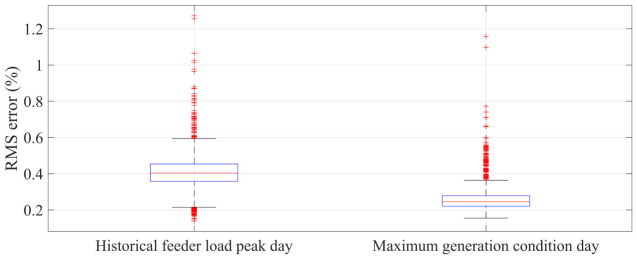

FIGURE 12. For the two scenarios considered, the RMS errors calculated over one day between the field-measured voltages and the voltages obtained from the enhanced OpenDSS model for all the voltage meters in the system are plot using a box and whisker plot. The red line in the middle in each case indicates the median error, the box indicates the interquartile range, and the whiskers are defined as 1.5 times the interquartile range away from the box.

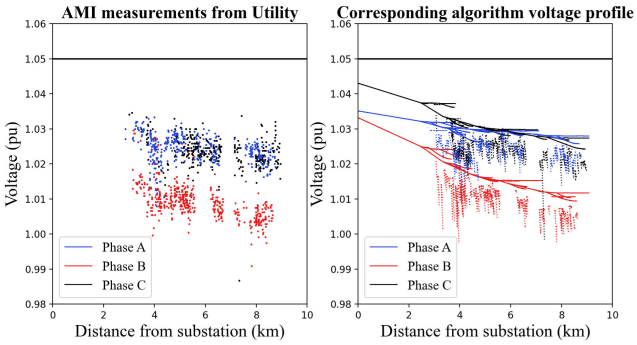

FIGURE 13. AMI measurements from the utility compared against the corresponding voltage profile obtained from the enhancement algorithm for the historical feeder load peak.

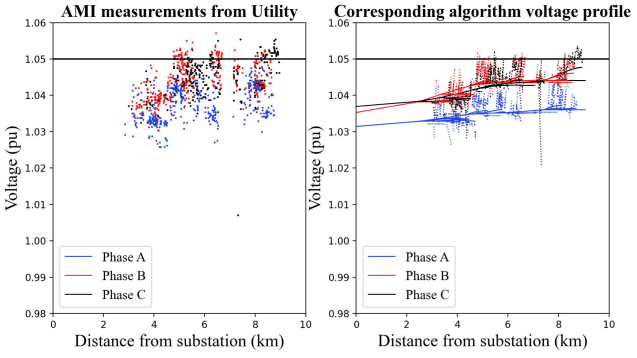

FIGURE 14. AMI measurements from the utility compared against the corresponding voltage profile obtained from the enhancement algorithm for the maximum generation condition.

historical feeder peak load day and maximum generation condition day are shown in Fig. 10 and Fig. 11, respectively. The distances from the substation of the locations corresponding to the plot are shown above each plot. The RMS error over a day is also calculated for all the meters along the feeder. Fig. 12 shows the *RMS* error calculated over a day for both days in a box-and-whisker plot. As observed, the average

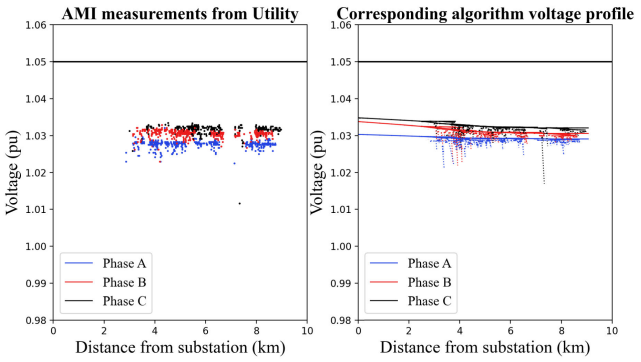

FIGURE 15. AMI measurements from the utility compared against the corresponding voltage profile obtained from the enhancement algorithm during the night.

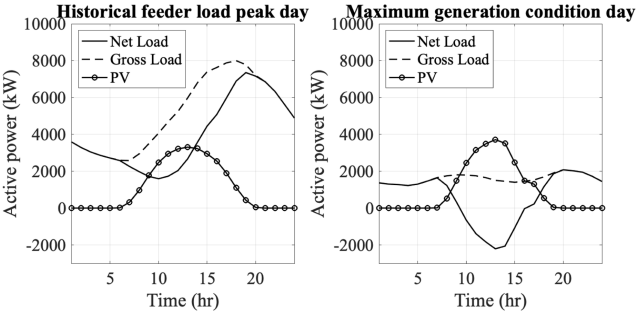

FIGURE 16. Distribution Feeder Gross load, net load, and PV production behavior.

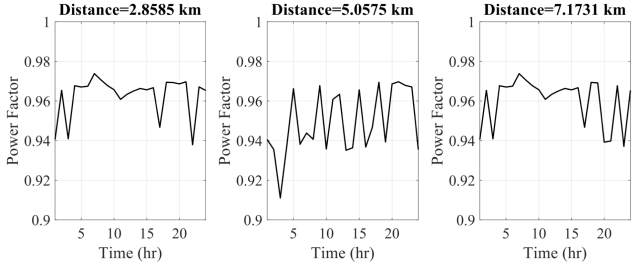

FIGURE 17. Power factor for some premises along the feeder for the historical feeder load peak day.

RMS error along the feeder length is around 0.4%, for the historical feeder load peak day and 0.2% for the maximum generation condition day, which shows that the proposed method achieves a very good match when compared against field measurements and that the enhanced feeder model accurately represents the actual field measurements.

Fig. 13, 14 and 15, show the AMI measurements received from the utility compared against the corresponding voltage profile obtained from the enhancement algorithm for three different snapshot conditions - historical feeder load peak, the maximum generation condition, and during the night (no PV production). The method proposed provides a complete power flow solution for both the primary and the secondary sides by using sparse measurements at the secondary

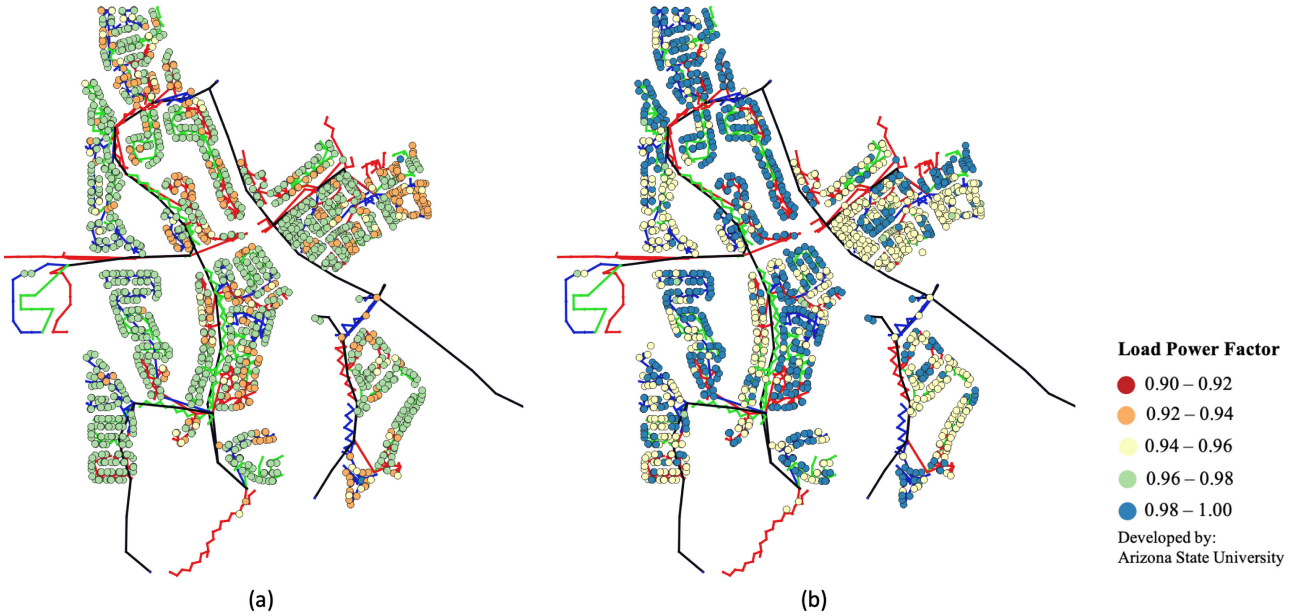

FIGURE 18. Customers' power factors obtained from the enhanced feeder model for all the loads in the feeder for both cases, the historical feeder load peak snapshot (a) and the maximum generation condition snapshot (b).

level along the feeder, extending the observability and planning capabilities of the feeder under study.

V. DETAILED FEEDER CHARACTERISTICS

This section presents some feeder characteristics derived from the enhanced feeder model developed. Fig. 16 shows the gross load, net-load, and PV production for the historical feeder load peak day and maximum generation condition day. For the maximum generation condition day, it is seen that the PV production significantly impacts the net load of the system. In this case, due to the significant penetration of solar PV, the net load is negative between 10 AM − 3 PM. Hence there is a large reverse active power flow from this feeder during this time. Due to this behavior, the feeder experiences large overvoltage during this time. The maximum solar PV generation occurs around 1 PM. The voltage profile for this time is shown in Fig. 14, showing a trend of increasing magnitude moving away from the substation due to the reverse active power flow as well as the capacitive nature of the distribution cables. Note that the unbalance between the phases in the feeder is successfully captured by the optimization-based technique proposed.

As shown in Fig. 16, the historical feeder load peak day has a high load, which is why there is no reverse flow at the feeder-head – there is still a significant reduction in the net load due to solar PV production. In Fig. 13, the voltage profile of the feeder corresponding to an evening condition (high load) for the historical feeder load peak day shows a decreasing trend as we go away from the substation, which is traditionally expected for distribution systems. Fig. 15 shows a power flow snapshot at night (2 AM) on the maximum generation day. In this case, because of the absence of solar PV generation and the presence of light load, the voltage profile does not experience a large change as compared with the other two cases.

The contrast in the feeder voltage profiles between the snapshots presented in Fig. 13, 14 and 15 as well as the gross and net loads presented in Fig. 16 highlight the fact that a distribution system with a high solar PV penetration can exhibit a wide range of behaviors, hence accurately modeling the distribution system is important for any studies involving it.

Fig. 17 shows the power factor for some premises along the feeder for the historical feeder load peak day. The enhancement algorithm estimates the power factor for each load independently. Fig. 18 shows the customers power factor obtained from the enhanced feeder model for all the loads in the feeder for both cases, the historical feeder load peak snapshot (a) and the maximum generation condition snapshot (b). The difference in the two cases is reflected in the different power factor levels – the power factors for the load peak are lower than the maximum generation condition, due to the high load demand.

VI. DISCUSSION

Using the method proposed in this paper, accurate and detailed primary and secondary distribution system models can be created for distribution feeder analyses using sparse field measurements. An accurate and detailed feeder model is essential to capture the behavior of distribution feeders for various studies such as snapshot/dynamic hosting capacity, snapshot/dynamic impact analysis, distribution system integration costs of renewables analysis, as well as to capture voltage and thermal violations accurately and to

efficiently manage renewable energy sources with advanced Volt/VAr optimization and other distribution system automation schemes.

The proposed method assumes that the network topology, line impedances, and field measurements, i.e., AMI/DAS/SCADA measurements, are known and accurate. Using these measurements, the optimization-based method estimates the reactive power demand for all the loads in the feeder – no reactive power measurements are necessary along the feeder but can be added to the model as parameters if available, as well as the active power demands for the unmetered loads.

In the absence of load reactive power measurements, the method uses other available measurements such as active power and voltage measurements to calculate the active and reactive powers, i.e., power factor, for the loads. Since the reactive power/power factor is estimated based on the available field measurements of active power and voltage, the resulting model is more accurate than a model constructed with the assumption of a single power factor for all the loads. However, a possible source of inaccuracies is any potential inconsistency arising due to different possible methods of measuring various quantities (e.g., instantaneous value versus moving average).

As discussed in Section IV, the proposed method takes 32 seconds to enhance the feeder model for one snapshot for the selected distribution feeder. Hence, this method is suitable for planning studies where a detailed model of the feeder is desired. The enhanced feeder model can be updated for operational analyses conducted once every minute/few minutes. It is worth noting that the AMI measurements may update only a few times an hour - or even a few times a day. Therefore, the proposed method is suitable to continuously calculate a detailed and accurate feeder model for each system status.

VII. CONCLUSION

To accurately represent the distribution systems in studies, constructing a detailed model which corresponds to the actual feeder(s) is essential. This paper describes a novel procedure to enhance the model of a real distribution system feeder using AMI and DAS data. This novel enhancement algorithm formulates an ACOPF based on IV formulation for matching the voltages at various nodes to AMI measurements, ensuring that the tuned model closely reflects the real-life status of the feeder for a snapshot. The model is validated using time-series analysis in OpenDSS. Simulation results for voltages have an average RMS error along the feeder under 0.5%, and all RMS errors are under 1.4% compared to the field measurements providing confidence in the developed method. In the future, this modeling procedure can be used to create comprehensive databases for further analysis and study of the distribution networks when no AMI data is available to construct the profiles and hence guide future extensions to the distribution systems.

REFERENCES

[1] B. Kroposki *et al.*, "Autonomous energy grids: Controlling the future grid with large amounts of distributed energy resources," *IEEE Power Energy Mag.*, vol. 18, no. 6, pp. 37–46, Nov. 2020. [Online]. Available: https://ieeexplore.ieee.org/document/9229208/

[2] R. Quint *et al.*, "Transformation of the grid: The impact of distributed energy resources on bulk power systems," *IEEE Power Energy Mag.*, vol. 17, no. 6, pp. 35–45, Nov. 2019.

[3] T. Gonen, *Electric Power Distribution Engineering*, vol. 3, no. 2. Boca Raton, FL, USA: CRC Press, Aug. 2015.

[4] W. H. Kersting, *Distribution System Modeling and Analysis*, 4th ed. Boca Raton, FL, USA: CRC Press, Aug. 2017. [Online]. Available: https://www.taylorfrancis.com/books/9781498772143

[5] J. Guerrero *et al.*, "Distributed generation: Toward a new energy paradigm," *IEEE Ind. Electron. Mag.*, vol. 4, no. 1, pp. 52–64, Mar. 2010. [Online]. Available: https://ieeexplore.ieee.org/document/5439058/

[6] F. Bu, Y. Yuan, Z. Wang, K. Dehghanpour, and A. Kimber, "A time-series distribution test system based on real utility data," in *Proc. North Amer. Power Symp. (NAPS)*, 2019, pp. 1–6, doi: 10.1109/NAPS46351.2019.8999982.

[7] Y. Tang and R. Ayyanar, "Modeling and validation of a distribution system with high PV penetration using zone division method," in *Proc. IEEE Power Eng. Soc. Transmiss. Distrib. Conf.*, Apr. 2014, pp. 1–5. [Online]. Available: https://ieeexplore.ieee.org/document/6863357/

[8] T. J. Morrell, V. Venkataramanan, A. Srivastava, A. Bose, and C. Liu, "Modeling of electric distribution feeder using smart meter data," in *Proc. IEEE/PES Transmiss. Distrib. Conf. Expo. (T&D)*, 2018, pp. 1–9, doi: 10.1109/TDC.2018.8440540.

[9] J. Giraldez, P. Gotseff, A. Nagarajan, R. Ueda, J. Shindo, and S. Suryanarayanan, "Distribution feeder modeling for time-series simulation of voltage management strategies," *Proc. IEEE Power Eng. Soc. Transmiss. Distrib. Conf.*, Apr. 2018, pp. 2–6.

[10] J. A. Taylor, T. A. Short, and B. Bushey, "Efficiency impacts of distribution secondaries," *Proc. IEEE Power Eng. Soc. Transmiss. Distrib. Conf.*, May 2012, pp. 1–6.

[11] J. Peppanen, M. J. Reno, M. Thakkar, S. Grijalva, and R. G. Harley, "Leveraging AMI data for distribution system model calibration and situational awareness," *IEEE Trans. Smart Grid*, vol. 6, no. 4, pp. 2050–2059, Jul. 2015. [Online]. Available: https://ieeexplore.ieee.org/document/7010947/

[12] J. Peppanen, M. J. Reno, R. J. Broderick, and S. Grijalva, "Distribution system model calibration with big data from AMI and PV inverters," *IEEE Trans. Smart Grid*, vol. 7, no. 5, pp. 2497–2506, Sep. 2016. [Online]. Available: https://ieeexplore.ieee.org/document/7426397/

[13] Y. Tang, X. Mao, and R. Ayyanar, "Distribution system modeling using CYMDIST for study of high penetration of distributed solar photovoltaics," in *Proc. North Amer. Power Symp.*, Sep. 2012, pp. 1–6. [Online]. Available: https://ieeexplore.ieee.org/document/6336408/

[14] Y. Tang and R. Ayyanar, "Methodology of automated protection analysis for large distribution feeders with high penetration of photovoltaic systems," *IEEE Power Energy Technol. Syst. J.*, vol. 4, no. 1, pp. 1–9, Mar. 2017. [Online]. Available: https://ieeexplore.ieee.org/document/7493637/

[15] B. Wang and W. Luan, "Generate distribution circuit model using AMI data," in *Proc. China Int. Conf. Electr. Distrib. (CICED)*, Sep. 2014, pp. 1251–1255.

[16] Y.-F. Huang, S. Werner, J. Huang, N. Kashyap, and V. Gupta, "State estimation in electric power grids: Meeting new challenges presented by the requirements of the future grid," *IEEE Signal Process. Mag.*, vol. 29, no. 5, pp. 33–43, Sep. 2012.

[17] Z. Soltani, S. Ma, M. Khorsand, and V. Vittal, "Simultaneous robust state estimation, topology error processing, and outage detection for unbalanced distribution systems," 2021, *arXiv:2105.10111*.

[18] EPRI. (2019). *OpenDSS—EPRI Distribution System Simulator*. [Online]. Available: https://smartgrid.epri.com/SimulationTool.aspx

[19] K. Montano-Martinez, S. Thakar, V. Vittal, R. Ayyanar, and C. Rojas, "Detailed primary and secondary distribution system feeder modeling based on AMI data," in *Proc. 52nd North Amer. Power Symp. (NAPS)*, Apr. 2021, pp. 1–6.

[20] K. Montano and S. Thakar. (2020). *DISMOTT: Distribution System Model Transformation Tool*. [Online]. Available: https://github.com/thakars/DISMOTT

[21] W. E. Hart *et al.*, *Pyomo—Optimization Modeling in Python* (Springer Optimization and Its Applications), vol. 67. Cham, Switzerland: Springer, 2017, doi: 10.1007/978-3-319-58821-6.
[22] W. E. Hart, J.-P. Watson, and D. L. Woodruff, "Pyomo: Modeling and solving mathematical programs in Python," *Math. Program. Comput.*, vol. 3, no. 3, pp. 219–260, 2011, doi: 10.1007/s12532-011-0026-8.
[23] A. Wächter and L. T. Biegler, "On the implementation of an interior-point filter line-search algorithm for large-scale nonlinear programming," *Math. Program.*, vol. 106, no. 1, pp. 25–57, May 2006, doi: 10.1007/s10107-004-0559-y.
[24] R. P. O'Neill, A. Castillo, and M. B. Cain, "The IV formulation and linear approximations of the AC optimal power ow problem," FERC, Washington, DC, USA, FERC Staff Paper–Optim. Power Flow Paper 2, Dec. 2012. Accessed: Nov. 2021. [Online]. Available: https://www.ferc.gov/sites/default/files/2020-05/acopf-2-iv-linearization.pdf
[25] D. K. Molzahn *et al.*, "A survey of distributed optimization and control algorithms for electric power systems," *IEEE Trans. Smart Grid*, vol. 8, no. 6, pp. 2941–2962, Nov. 2017.
[26] T. A. Short, "Advanced metering for phase identification, transformer identification, and secondary modeling," *IEEE Trans. Smart Grid*, vol. 4, no. 2, pp. 651–658, Jun. 2013.

KAREN MONTANO-MARTINEZ (Graduate Student Member, IEEE) received the B.Sc. degree in electrical engineering and the B.Sc. degree in electronics engineering from Universidad del Norte, Barranquilla, Colombia, in 2015 and 2016, respectively, and the M.Sc. degree in power systems from the University of Puerto Rico, Mayaguez, PR, USA, in 2019. She is currently pursuing the Ph.D. degree in electrical engineering with Arizona State University, Tempe, AZ, USA.

SUSHRUT THAKAR (Graduate Student Member, IEEE) received the B.Tech. degree in energy science and engineering and the M.Tech. degree in energy systems engineering from IIT Bombay, Mumbai, India, in 2018. He is currently pursuing the Ph.D. degree with the School of Electrical, Computer and Energy Engineering, Arizona State University, Tempe, AZ, USA.

SHANSHAN MA (Member, IEEE) received the B.S. degree in information and electrical engineering from the Zhejiang University City College, Hangzhou, China, in 2012, the M.S. degree from the Department of Electrical Engineering and Computer Science, South Dakota State University, Brookings, SD, USA, in 2015, and the Ph.D. degree from the Department of Electrical and Computer Engineering, Iowa State University, Ames, IA, USA, in 2020. She is currently a Postdoctoral Research Scholar with the School of Electrical, Computer and Energy Engineering, Arizona State University, Tempe. Her current research interests include optimization and control in power distribution systems.

ZAHRA SOLTANI (Graduate Student Member, IEEE) is currently pursuing the Ph.D. degree in electrical engineering with Arizona State University, Tempe, USA. Her research interests include distributed energy resources (DERs) modeling and scheduling, and power system operation, including topology processor and state estimation.

VIJAY VITTAL (Life Fellow, IEEE) received the Ph.D. degree from Iowa State University, Ames, in 1982. He is currently a Regents' Professor and the Ira A. Fulton Chair Professor with the School of Electrical, Computer and Energy Engineering, Arizona State University, Tempe. He is a member of the National Academy of Engineering.

MOJDEH KHORSAND (Member, IEEE) received the B.Sc. degree in electrical engineering from the University of Mazandaran, Iran, in 2007, the M.Sc. degree in electrical engineering from the Iran University of Science and Technology, Tehran, Iran, in 2010, and the Ph.D. degree in electrical engineering from Arizona State University, Tempe, AZ, USA, in 2017. She is currently an Assistant Professor with the School of Electrical, Computer and Energy Engineering, Arizona State University. Her research interests include power system operations, electric energy markets, transient stability, and protection systems.

RAJAPANDIAN AYYANAR (Senior Member, IEEE) received the M.S. degree in power electronics from the Indian Institute of Science, Bengaluru, India, in 1995, and the Ph.D. degree in power electronics from the University of Minnesota, Minneapolis, MN, USA, in 2000. He is currently a Professor with Arizona State University, Tempe, AZ, USA.

CYNTHIA ROJAS (Member, IEEE) received the B.Sc. degree in electrical and electronics engineering from New Mexico State University, NM, USA, in 2014. She is currently an Engineer III in distributed resources engineering with Arizona Public Service (APS).